This is the peer-reviewed, final accepted version for American Mineralogist, published by the Mineralogical Society of America.
The published version is subject to change. Cite as Authors (Year) Title. American Mineralogist, in press.
DOI: https://doi.org/10.2138/am-2020-7264. http://www.minsocam.org/

Revision 3

Water quantification in olivine and wadsleyite by Raman spectroscopy and study of errors and uncertainties

MARTINEK LOÏS[1] AND BOLFAN-CASANOVA NATHALIE[1]

[1]Laboratoire Magmas et Volcans, 6 avenue Blaise Pascal, TSA 60026 – CS 60026, 63178 Aubière Cedex

ABSTRACT

The study of nominally anhydrous minerals with vibrational spectroscopy, despite its sensitivity, tends to produce large uncertainties (in absorbance or intensity) if the observed dispersion of the values arising from the anisotropy of interaction with light in non-cubic minerals is not assessed. In this study, we focused on Raman spectroscopy, which allows the measurement of crystals down to few micrometers in size in back-scattered geometry, and with any water content, down to 200 ppm by weight of water. Using synthetic hydrous single-crystals of olivine and wadsleyite, we demonstrate that under ideal conditions of measurement and sampling, the data dispersion reaches ±30% of the average (at 1σ) for olivine, and ±32% for wadsleyite, mostly because of their natural anisotropy. As this anisotropy is linked to physical properties of the mineral, it should not be completely considered as error without treatment. By simulating a large number of measurements with a 3D model of the OH/Si spectral intensity ratio for olivine and wadsleyite as a function of orientation, we observe that although dispersion increases when increasing the number of measured points in the sample, analytical error decreases, and the contribution of anisotropy to this error decreases. With a sufficient number of

Always consult and cite the final, published document. See http:/www.minsocam.org or GeoscienceWorld

This is the peer-reviewed, final accepted version for American Mineralogist, published by the Mineralogical Society of America.
The published version is subject to change. Cite as Authors (Year) Title. American Mineralogist, in press.
DOI: https://doi.org/10.2138/am-2020-7264. http://www.minsocam.org/

points (five to ten, depending on the measurement method), the greatest contribution to the error on the measured intensities is related to the instrument's biases, and reaches 12 to 15% in ideal cases, indicating that laser and power drift corrections have to be carefully performed. We finally applied this knowledge on error sources (to translate data dispersion into analytical error) on olivine and wadsleyite standards with known water contents to build calibration lines for each mineral in order to convert the intensity ratio of the water bands over the structural bands (OH/Si) to water content. The conversion factor from OH/Si to ppm by weight of water (H_2O) is 93108±24005 for olivine, 250868±45591 for iron-bearing wadsleyite, and 57546±13916 for iron-free wadsleyite, showing the strong effect of iron on the spectral intensities.

Keywords: wadsleyite, olivine, nominally anhydrous minerals, Raman spectroscopy, water quantification

INTRODUCTION

Even though the major mineral phases of the Earth's mantle are nominally anhydrous, many of them are known to contain water as OH point defects in their structure (Bell and Rossman, 1992; Smyth and Keppler, 2006; Peslier 2010; Demouchy & Bolfan-Casanova, 2016). The water storage capacity of the most abundant upper mantle mineral, namely olivine, has been the subject of many studies, however most reports concern simple systems or single crystal olivine (e.g. Kohlstedt et al. 1996; Withers & Hirschmann 2007 and 2008; Bali et al. 2008; Kovács et al. 2010; Férot & Bolfan-Casanova 2012; Litasov et al. 2014, Yang et al. 2016). Single-phase experiments allow the growth of single crystals large enough to be suitable for any analytical method, especially absorption infrared spectroscopy using Fourier transform infrared (FTIR), secondary ion mass spectrometry (SIMS), or elastic recoil detection analysis (ERDA).

Always consult and cite the final, published document. See http:/www.minsocam.org or GeoscienceWorld

This is the peer-reviewed, final accepted version for American Mineralogist, published by the Mineralogical Society of America.
The published version is subject to change. Cite as Authors (Year) Title. American Mineralogist, in press.
DOI: https://doi.org/10.2138/am-2020-7264. http://www.minsocam.org/

In experiments with natural mantle compositions on the other hand, olivine, orthopyroxene, clinopyroxene and garnet can coexist, strongly limiting crystal growth. These samples often display crystal sizes from 20 to 50 μm, limiting the use of the conventional methods cited above on the fine-grained samples. Investigation of the storage capacity in more complex systems such as peridotite has been carried out and the small grain size of the grains required the use of SIMS (few tens of cubic micrometers analyzed) or even nano-SIMS (one or two order of magnitude less) (see Ardia et al., 2012; Tenner et al., 2012; Novella et al., 2014). This technique is complicated to use because of high background levels of H, complex preparation to avoid H contamination and the need for well-characterized standards (Koga et al. 2003, Mosenfelder et al. 2011).

FTIR is frequently used sensitive technique to quantify hydroxyl content in nominally anhydrous minerals, which also gives structural information about H point defects. Reliable methods exist to quantify water in anisotropic minerals using FTIR, and a consequent literature exists on the subject (e.g., Libowitzsky and Rossman 1996; Asimow et al. 2006; Kovács et al. 2008; Withers et al. 2012, Withers 2013; Qiu et al. 2018). However, in the case of very water-rich samples as, for example, wadsleyite, a high-pressure polymorph of olivine, that can contain up to 3.2 weight percent of water (Inoue et al., 1995), infrared spectroscopy requires an important thinning of the samples (which may cause their loss) in order to avoid the entire absorption of the infrared signal.

In this study, we used confocal polarized Raman spectroscopy (the laser source being polarized, the incident beam is therefore also polarized). This technique offers several advantages for water quantification in synthetic minerals with a small grain size and low to very high water contents. Regarding sample preparation, OH quantification using back-scattered Raman

Always consult and cite the final, published document. See http:/www.minsocam.org or GeoscienceWorld

spectroscopy requires only one side of the sample to be polished, while double polishing is required in the measurement of absorbance using FTIR. Unfortunately, very thin polishing of the sample can irremediably damage them, especially those sintered under conditions where fluids are highly wetting, which is the case of the conditions of the deep upper mantle (Yoshino et al. 2007). The detection limit of water quantification using Raman spectroscopy (around 50-100 ppm wt) may be a problem with samples synthesized under conditions of the uppermost mantle, where the water solubility is the lowest for many mineral species (Férot & Bolfan-Casanova 2012, Yang 2016), but any higher concentration can be measured (Bolfan-Casanova et al. 2014). The spot size of confocal Raman spectroscopy (3-5 μm) allows measurements on very fine-grained samples (down to crystal sizes around 5 μm) without difficulties. The time required for reasonably precise measurements (some minutes) is low enough to multiply the number of measured points on different crystals throughout the sample and have a statistically correct coverage of the whole sample. One major drawback of Raman spectroscopy is that the intensity absorption depends on many factors in addition to the concentration, such as the intensity of the incident laser, confocality and lens magnification, which control the volume of sample that is excited by the laser beam. Moreover, the chosen gratings and the optics of the spectrometer (instrument-dependent parameters), as well as the optical properties of the sample or its surface state will affect the efficiency of the measurement (see e.g. Mercier et al. 2009, Schiavi et al. 2018; Zarei et al. 2018). In contrast, the absorbance measured using FTIR depends solely on the thickness, concentration and absorptivity of the sample itself, following a relationship known as the Beer-Lambert law. In addition, in absorbance spectroscopy the intensity transmitted by the sample is always normalized to that of the incident beam, which tends to eliminate instrumental biases on the intensity of the signal from the sample.

Always consult and cite the final, published document. See http:/www.minsocam.org or GeoscienceWorld

This is the peer-reviewed, final accepted version for American Mineralogist, published by the Mineralogical Society of America.
The published version is subject to change. Cite as Authors (Year) Title. American Mineralogist, in press.
DOI: https://doi.org/10.2138/am-2020-7264. http://www.minsocam.org/

89 Raman spectroscopy is widely used to quantify H_2O concentrations in glasses or melt
90 inclusions (e.g., Thomas et al. 2008; Mercier et al. 2009; Schiavi et al., 2018). In these studies,
91 quantification of the water concentration relies on the comparison of the OH/Si of the unknown
92 to that of well-characterized standards measured under identical conditions, as the OH intensity
93 has been shown to increase linearly with water content. Here, OH/Si is defined by the integrated
94 intensity of the water band normalized to that of the silicate vibrations (see the following section
95 for details). As numerous factors may affect the measurement efficiency (such as variation of
96 focusing depth or surface quality), using the ratio of the OH band area over that of silica bands
97 area reduces the data dispersion or scatter, as both regions are equally affected by focusing or
98 surface variations. Calibrations of the method have been proposed by Thomas et al. (2008 and
99 2015) for garnet, Bolfan-Casanova et al. (2014) for olivine, Thomas et al. (2015) for ringwoodite,
100 and Weis et al. (2018) for orthopyroxene (this last study having used also forward-scattering).

101 Previous water content quantification in olivine conducted with Raman spectroscopy
102 often display large error bars on their results (Bolfan-Casanova et al. 2014). In this study, we
103 demonstrate that those error bars are significantly related to the dispersion (used in the statistical
104 meaning of the term throughout this work) of the relative intensities of the different vibrational
105 modes caused by the anisotropy of the minerals. As this anisotropy is a natural consequence of
106 the structure and symmetry of the crystal, it is not directly related to error, and can even be used
107 to get information on orientation (see for example Ishibashi et al. 2008). Firstly, we studied the
108 relative effect of the different error sources and of anisotropy on the statistical dispersion of
109 measurements in hydrated olivine and wadsleyite single crystals and used it to propose a method
110 to estimate the analytical error from the data dispersion of the measurements using polarized

Always consult and cite the final, published document. See http:/www.minsocam.org or GeoscienceWorld

This is the peer-reviewed, final accepted version for American Mineralogist, published by the Mineralogical Society of America.
The published version is subject to change. Cite as Authors (Year) Title. American Mineralogist, in press.
DOI: https://doi.org/10.2138/am-2020-7264. http://www.minsocam.org/

111 unanalyzed Raman spectroscopy. We then propose a calibration for water quantification in
112 olivine and wadsleyite based on standards characterized by FTIR or ERDA methods.

113 # METHODS

114 ## Synthesis of olivine and wadsleyite

115 Olivine and wadsleyite single crystals were synthesized in the multi-anvil press at 12 and
116 15 GPa and at 1200 and 1350 °C from San Carlos olivine as starting material. Olivine single
117 crystals and powder were placed in a folded rhenium foil capsule, placed itself in a welded gold-
118 palladium capsule containing brucite powder. The experimental assembly consisted of an MgO
119 octahedron containing Cr_2O_3, a zirconia thermal insulator, a $LaCrO_3$ heater with molybdenum
120 electrodes in contact with the anvils and an MgO central part containing the capsule. Temperature
121 was controlled using a W-Re thermocouple (5% and 26% Re). Experiments were conducted at
122 the Laboratoire Magmas et Volcans (LMV, Clermont-Ferrand, France) on a Voggenreiter Mavo-
123 press LP 1500 tons multi-anvil press equipped with a Kawai-Endo apparatus. Heating was
124 performed and controlled by a Pacific 140-AMX AC power source. Secondary anvils were 32
125 mm tungsten carbide cubes with 8 and 6 mm truncations. Olivine synthesis duration was 4.5
126 hours at 1200 °C, and wadsleyite synthesis lasted 2 hours at 1350 °C. For both syntheses,
127 temperature was gradually decreased after the experiment (around 50 °C per minute) instead of
128 quenching to prevent crystal fracturation. Recovered crystals were oriented using polarized light
129 microscopy for olivine and X-ray diffraction for wadsleyite, and then cut and mirror polished
130 perpendicular to crystallographic axes (see Figure 1). Olivine and wadsleyite are both
131 orthorhombic so display an anisotropic behavior with respect to light absorption. Wadsleyite has
132 been reported to become monoclinic above 0.5 wt % H_2O using X-ray diffraction (Jacobsen et al.

Always consult and cite the final, published document. See http:/www.minsocam.org or GeoscienceWorld

2005), however we did not detect any noticeable spectral difference that could be due to this small change in the β-angle.

FTIR spectroscopy

Most of the samples used in order to calibrate the Raman quantification method were olivines characterized using FTIR by Férot & Bolfan-Casanova (2012). These water content values were updated using the most recent calibration of the infrared extinction coefficient (ε) determined using ERDA by Withers et al. (2012) of 45200 l $mol_{H_2O}^{-1}$ cm^{-2} instead of the 28450 l $mol_{H_2O}^{-1}$ cm^{-2} value given by Bell et al. (2003). This decreases all the water contents of olivine reported in Férot and Bolfan-Casanova (2012) by a factor of 1.589.

Polarized spectra acquired for this study were collected on a Vertex70 Brucker spectrometer coupled to a Hyperion microscope with a 15× lens, condenser and knife-edge apertures creating a rectangular target area of 40-50 µm. Samples were analyzed on a CaF_2 plate at a resolution of 2 cm^{-1}, with 200 to 300 accumulations. After background subtraction and atmospheric correction, a cubic baseline correction has been applied on the 1500 to 4000 cm^{-1} area, and integration calculated in the 2700 to 3720 cm^{-1} area. The absorbance is then used to calculate the H_2O content based on Beer Lambert's law (see equation 1) with the integrated molar absorption coefficient (also called extinction coefficient) cited above, and a density factor X of 5521 $l \cdot mol_{H_2O}^{-1}$ (used to convert $mol_{H_2O} \cdot l^{-1}$ to ppm by weight of H_2O, equal to $18.02 \times 10^6/\rho$). The density ρ has been calculated from Fischer & Medaris (1969) accounting for the olivine composition. The equation used is the following, with ε being the infrared extinction coefficient, A_{tot} the total absorbance, and d the thickness of the sample in centimeters:

Always consult and cite the final, published document. See http:/www.minsocam.org or GeoscienceWorld

This is the peer-reviewed, final accepted version for American Mineralogist, published by the Mineralogical Society of America.
The published version is subject to change. Cite as Authors (Year) Title. American Mineralogist, in press.
DOI: https://doi.org/10.2138/am-2020-7264. http://www.minsocam.org/

Equation 1

$$C_{H_2O} = X \times \frac{A_{tot}}{\varepsilon \times d}$$

Raman spectroscopy

Raman spectra were collected at LMV using an InVia confocal Raman micro-spectrometer manufactured by Renishaw and equipped with a 532 nm diode laser (200 mW output power), a Peltier-cooled CCD detector of 1024×256 pixels, a motorized XYZ stage and a Leica DM 2500M optical microscope. Scattered light was collected in a back-scattered geometry. An edge filter effectively reduced both Rayleigh scattered photons and photons from the exciting laser source at 0 cm^{-1} that had been reflected by the sample surface. A 2400 grooves/mm grating was used for the analyses, which resulted in a spectral resolution between 1.3 cm^{-1} (around 100 cm^{-1}) and 0.72 cm^{-1} (around 3700 cm^{-1}). All spectra were acquired with polarized light without analyzer, and sample was rotated under the beam to change the polarization angle. A ×100 microscope lens (numerical aperture 0.9) was used and the slit aperture was set to 20 μm (high confocality setting). Daily calibration of the spectrometer was performed based on a Si 520.5 cm^{-1} peak. The effective laser power (changed by filters) used was 65 to 71 mW for olivine, and 8 to 9 mW for wadsleyite and glass (low enough power to prevent destabilization and dehydration) and was measured to normalize spectra to 1 mW. A power of 125 to 140 mW can cause some damages on water-rich olivine, and a power of 15 mW caused a slight OH intensity reduction in wadsleyite with very high water content (sample 2054, 3.4% in weight), but no dehydration or destabilization effect has been observed with the lower laser power values finally chosen. A hydrous basaltic glass (see Schiavi et al. 2018) is used to check and be able to correct for power drifts and efficiency drifts along the different area of measurement.

Always consult and cite the final, published document. See http:/www.minsocam.org or GeoscienceWorld

This is the peer-reviewed, final accepted version for American Mineralogist, published by the Mineralogical Society of America.
The published version is subject to change. Cite as Authors (Year) Title. American Mineralogist, in press.
DOI: https://doi.org/10.2138/am-2020-7264. http://www.minsocam.org/

As already stated above, the quantification of water concentration is based on the measurement of the OH band integrated intensity normalized to the silicate band integrated intensity. Under static conditions of measurement, the window analyzed using a grating of 2400 groves/mm decreases from approximately 1200 cm^{-1} at low wavenumbers to 800 cm^{-1} at high wavenumbers. For all samples and standards, Si area refers to wavenumbers from 61 to 1318 cm^{-1} centered on 720 cm^{-1}, and OH area refers to wavenumbers from 2978 to 3784 cm^{-1} centered on 3400 cm^{-1}. Both areas were chosen to contain all the needed peaks and bands. Acquisition times are short for the Si area because of its high intensity, to prevent saturation of the CCD detector, and longer for the OH area to increase the signal to noise ratio, the OH bands being much weaker. Thus, acquisition times were 2×5 s for the Si area, and 5×60 s for the OH area of olivine and wadsleyite. For the glass, the acquisition times were 4×10 s for the Si area, and 5×120 s for the OH area. The daily variations of the spectrometer were corrected by normalizing to the average OH/Si intensity ratio of the hydrated glass measured in each measurement session, each of those consisting on two random points on the glass sample, providing a more reproducible OH/Si intensity ratio here called $(OH/Si)_{Smp\_Norm}$. The normalization operation is shown in equation 2, where $(OH/Si)_{Smp\ Meas}$ is the average OH/Si of the measured sample, $(OH/Si)_{Glass\_Meas}$ is the standard glass OH/Si measured in the same session as the sample, and $(OH/Si)_{Glass\_Std}$ is the measurement of the OH/Si of the glass measured in the same session as the standards. The result is the normalized OH/Si of the sample $(OH/Si)_{Smp\_Norm}$.

Equation 2

$$\frac{\mathrm{OH}}{\mathrm{Si}}_{Smp\ Norm} = \frac{\mathrm{OH}}{\mathrm{Si}}_{Smp\ Meas} \times \frac{\frac{\mathrm{OH}}{\mathrm{Si}}_{Glass\ Std}}{\frac{\mathrm{OH}}{\mathrm{Si}}_{Glass\ Meas}}$$

Always consult and cite the final, published document. See http:/www.minsocam.org or GeoscienceWorld

This is the peer-reviewed, final accepted version for American Mineralogist, published by the Mineralogical Society of America.
The published version is subject to change. Cite as Authors (Year) Title. American Mineralogist, in press.
DOI: https://doi.org/10.2138/am-2020-7264. http://www.minsocam.org/

The procedure of baseline correction is essential in obtaining reproducible values of OH/Si for each phase (see Figure 2 and supplementary materials 1). The baseline shape is linear for the olivine Si area (rarely cubic), cubic for its OH area, cubic or polygonal for the wadsleyite Si area and cubic for its OH area. The anchor points used to define the baseline are shown in Figure 2. The spectra used afterwards for integrations are the raw spectra subtracted of the baseline, and divided by the total acquisition time and the laser power, to normalize each spectrum to a power of 1 mW and an acquisition time of 1 s. It has to be noted that this is not the unit of the spectra, as the intensity measured on each spectrum depends on various parameters of the instrument such as the grating and the wave number, but can be labelled as counts$\cdot s^{-1}\cdot mW^{-1}$. Integration consists in the area under the curve of the baseline-corrected and normalized spectrum: [200, 1100] for the Si area and [3050, 3700] for the OH area of olivine, and [300, 1100] for the Si area and [3150, 3700] for the OH area of wadsleyite (see Figure 2). The result of this integration defines thereafter the intensity of the spectra. In the case of wadsleyite, iron-bearing samples display a very intense band at 171 cm^{-1} that merges with the white line (at low wavenumbers) rendering its baseline correction unreliable due to the difficult anchoring of the baseline at low wavenumbers (see supplementary materials 1). This is why the integration of the Si area of wadsleyite starts at a higher wavenumber of 300 cm^{-1}.

For all the spectra of glass, the single-crystal spectra and some of the wadsleyite and olivine samples, one measurement point consists in the OH intensity divided by the Si intensity (OH/Si ratio) with the same polarization angle, and is referred as "single points". On most of the olivine and wadsleyite samples, one measurement point will be the average of two OH/Si ratio obtained from two measurements on the same crystal with orthogonal polarization angles, and is referred as "orthogonal couples".

Always consult and cite the final, published document. See http:/www.minsocam.org or GeoscienceWorld

This is the peer-reviewed, final accepted version for American Mineralogist, published by the Mineralogical Society of America.
The published version is subject to change. Cite as Authors (Year) Title. American Mineralogist, in press.
DOI: https://doi.org/10.2138/am-2020-7264. http://www.minsocam.org/

The averaged OH/Si values of several measurement points on a sample is the value used to compare the different samples. Eight olivine and seven wadsleyite standard samples of various known water contents have been used to build the calibration lines allowing the conversion from OH/Si ratio to water content. Water contents of olivine standards have been determined by FTIR, using Withers et al. (2012) extinction coefficient, and those of wadsleyite standards were measured by ERDA (Bolfan-Casanova et al. 2018).

RESULTS

Quantification of the OH/Si variation related to mineral orientation

In order to assess the effect of orientation alone on the dispersion of the average OH/Si value of each phase, polarized Raman spectra have been acquired on each face of the prepared single crystals of olivine and wadsleyite. We acquired 19 spectra, from 0 to 180°, on each face for both OH and Si area, and values for 190 to 350° were calculated by symmetry. Normalized OH/Si values were then fitted using equation 3 for olivine and equation 4 for wadsleyite (see Figure 3).

Equation 3

$$\frac{\mathrm{OH}}{\mathrm{Si}}(\theta) = H + a_1 \times \cos^2(\theta + d_1)$$

Equation 4

$$\frac{\mathrm{OH}}{\mathrm{Si}}(\theta) = H + a_1 \times \cos^2(\theta + d_1) + a_2 \times \cos^2(2 * (\theta + d_2))$$

Here, H is a constant depicting the minimum value for a given face adjusting the vertical position of the curve; a_1 is the amplitude (the difference between the maximum and minimum

Always consult and cite the final, published document. See http:/www.minsocam.org or GeoscienceWorld

intensities of the given face for equation 3) of the cosine describing the features with a period of 180° (2-fold symmetry) shifted of an angle d_1; a_2 is the amplitude of the cosine describing the features with a period of 90° (4-fold symmetry) shifted of an angle d_2. Each parameter has been optimized to minimize the differences between the measurement data and the fitted curve. It has to be noted that the necessity for introducing parameters d arise from the fact that crystals are not exactly polished following the crystallographic axes. These fits are thus empirical and only serve the purpose of creating a model of the analyzed crystals. For olivine, this misalignment is around 10° (as visible in Figure 3), and has later been neglected (the maxima of the faces (100) and (010) have been aligned along crystallographic axes in the 3D model). On the other hand, the misalignment of wadsleyite is high, and orientation has been lost, rendering necessary the use of the shift parameters *d*. The observed component with a 90° period is necessary in the case of wadsleyite to fit correctly the measured intensity, and can mostly be noticed in the fits of the intensity variations on the faces arbitrarily called F1, F2 and F3 (see M F1 and M F2 fit curves around 150 and 330°).

Considering that the single-crystal analyzed is homogeneous in water content, the only source of deviation between the modeled curve and the measured data is the combination of data treatment error and measurement error. Data treatment error has been estimated from the differences between repeated baseline correction and treatments of Raman spectra, and will be referred as E_{Tr} in following equations, tables and figures. The estimated values for E_{Tr} on OH/Si are 3.6% for olivine and 4.0% for wadsleyite. This error tends to remain small when the signal to noise ratio is high enough. The second error source taken into account is the one caused by all measurement uncertainties, such as surface irregularities or focus offset, and will be referred as E_{Meas}. Supposing that E_{Meas} and E_{Tr} are independent sources of error, the deviation of

Always consult and cite the final, published document. See http:/www.minsocam.org or GeoscienceWorld

measurement points from the model is the square root of the sum of the two error sources squared, and is provided by the fit shown in Figure 3. From this calculation, we obtain a measurement related uncertainty E_{Meas} reaching 4.4% for olivine, and 4.1% for wadsleyite. The last source of error arises from the daily variation of the spectrometer efficiency and the method used to correct it. Hence, the treatment and measurement errors related to this correction are the cause of an additional error of 11.9%, and will be referred as E_{Cor}. This value has been estimated accounting for the measurement and data treatment errors related to the standard glass measurement. The first two error, E_{Meas} and E_{Tr}, sources apply on each point separately, while the correction error E_{Cor} applies to all the points of a measurement session. The values of the estimated errors are reported in table 1.

The intensity versus angle model curves (as shown in Figure 3) were then used to build a 3D model of OH/Si variation as a function of crystallographic orientation. In Figure 3 it is visible that the fitted curves do not coincide with the corresponding minima and maxima from the other faces (for example, the maxima of the "a" and "b" curves for olivine are different, but both describe the OH/Si intensity parallel to the "c" axis and should be equal). These differences are very likely to be caused by misalignment of the polished faces with respect to the crystallographic axes. To obtain a continuous set of three curves in 3D (as depicted by the bold lines in Figure 4), the amplitudes of the curves have been increased or decreased so that they cross each other along the crystallographic axes, keeping at the same time the average value of each curve constant. Intermediate orientation values were completed by combining those acquired along crystallographic axes, each point of any orientation being obtained with equation 5:

Always consult and cite the final, published document. See http:/www.minsocam.org or GeoscienceWorld

This is the peer-reviewed, final accepted version for American Mineralogist, published by the Mineralogical Society of America.
The published version is subject to change. Cite as Authors (Year) Title. American Mineralogist, in press.
DOI: https://doi.org/10.2138/am-2020-7264. http://www.minsocam.org/

Equation 5

$$\left(\frac{OH}{Si}\right)_{\alpha} = \sum \left(\frac{OH}{Si}\right)_{i} \times \cos^2(\alpha_i)$$

In this equation, any orientation α is defined by a vector with a norm equal to the corresponding $(OH/Si)_{\alpha}$ value. This vector has one projection on each of the "a", "b" and "c" planes corresponding to values $(OH/Si)_i$ fitted with equation 3 or 4 for a given angle (see Figure 3). $(OH/Si)_{\alpha}$ is then calculated as being the sum of these three $(OH/Si)_i$, each multiplied by the squared cosine of the angle between the defined vector and its projection on the corresponding plane. This operation results in a peanut-shaped three-dimensional OH/Si model for each phase when displayed in a 3D polar graph (see Figure 4, depicting OH/Si variation in olivine and supplementary materials 2 for wadsleyite). The OH/Si is depicted here as the distance between the peanut-shaped surface and the intersection of the a, b, and c axes. In both olivine and wadsleyite cases, it can be observed that high OH/Si values are located along one axis, identified as the c-axis for olivine, and that variations seem approximately axisymmetric for both of them. This modelling process can be applied to other orthorhombic minerals (or quadratic), each model being based on its own measured OH/Si values (as shown in Figure 3). Minerals with other crystal system could still be modelled, but they might require a different procedure of polishing, measurement and 3D model extrapolation.

Distinguishing OH/Si natural dispersion and errors

The 3D OH/Si distribution models for olivine and wadsleyite have then been used as basis to simulate measurements, in order to untangle the effects of natural dispersion (i.e. due to crystallographic orientation) and analytical uncertainties on the final error for any type of measurement (single points or orthogonal couples) and as a function of the number of

Always consult and cite the final, published document. See http:/www.minsocam.org or GeoscienceWorld

This is the peer-reviewed, final accepted version for American Mineralogist, published by the Mineralogical Society of America.
The published version is subject to change. Cite as Authors (Year) Title. American Mineralogist, in press.
DOI: https://doi.org/10.2138/am-2020-7264. http://www.minsocam.org/

measurement points. To achieve this, the first step is to generate a set of random uniformly distributed crystal orientations that simulates a polycrystalline sample. A random "longitude" angle between 0 and 360° is first generated (uniform distribution), and a second "latitude" angle is generated with a semicircle distribution with a maximal probability for 0° and a probability of reaching zero when approaching 90 or -90°. To each orientation corresponds an OH/Si value determined as described for the construction of the 3D model. On each point chosen among those of this surface, the estimated measurement and treatment errors are applied, using equation 6. Here, X_{Meas} and X_{Tr} represent normally distributed random values with an average of zero, and a standard deviation equal to the desired error component E_{Meas} or E_{Tr}. Each "modeled", or simulated point $(OH/Si)_M$ has its own X_{Meas} and X_{Tr} values, because those errors do apply on every point separately and independently, finally yielding the "real" value $(OH/Si)_R$.

Equation 6

$$\frac{\mathrm{OH}}{\mathrm{Si}}_R = \frac{\mathrm{OH}}{\mathrm{Si}}_M \times (1 + X_{Meas}) \times (1 + X_{Tr})$$

For single point measurements, the simulated sample value will be the average of all the $(OH/Si)_R$, multiplied in the same way by $1 + X_{Cor}$ to simulate the errors arising from the laser power drift correction. In the case of orthogonal couples measurements, the two resulting $(OH/Si)_R$ values of each measurement point are averaged, then all points are again averaged before applying the $1 + X_{Cor}$ factor.

All the error and dispersion values used in the following section are expressed as relative errors, in percent of deviation from the average. Hereafter, the goal is to get the standard deviation and the average of each simulated measurement session for any number of measurement points and repeat the operation a large number of times to get a result as

Always consult and cite the final, published document. See http:/www.minsocam.org or GeoscienceWorld

statistically significant as possible. In this study, final values have been obtained for sets of 2 to 30 points in both single point and orthogonal couples, with one million draws for each case. For each number of points, the average of all the standard deviations of all sets of values has been interpreted as the expected measured dispersion D_{Th}, and the standard deviation of all the averages of all the set of points has been interpreted as the error expected for the measurement (E_{Th}). Both D_{Th} and E_{Th} depend on the number of measurement points and on the technique used for the measurement (single point or orthogonal couples). Dispersion increases when adding points, reaching an approximate plateau past 10 points, and error decreases when adding points, but stabilizes much slower past 30 points, limited by the contribution of E_{Cor} to the final error (see Figure 5).

The dispersion and error values obtained by the above simulation were then fitted to obtain error propagation equations as a function of the number of points, the measurement method, and the different errors sources. The natural dispersion caused by anisotropy can be estimated from equation 7 below. Here D_{Nat} is the natural dispersion, which is the expected relative standard deviation obtained on a random set of measurements without any kind of error added as a function of the number of points (N). D_{An} represents the total anisotropy, and is the same standard deviation as D_{Nat}, but for an infinite set of points, and finally "a" is a fitting parameter (all the values of the different parameters are shown in Table 1).

Equation 7

$$D_{Nat} = D_{An} - \frac{a}{N-1}$$

Equations 8 and 9 also express the dispersion of values and in addition takes into account the errors arising from measurement and data treatment. As the normalization related errors (E_{Cor})

Always consult and cite the final, published document. See http:/www.minsocam.org or GeoscienceWorld

This is the peer-reviewed, final accepted version for American Mineralogist, published by the Mineralogical Society of America.
The published version is subject to change. Cite as Authors (Year) Title. American Mineralogist, in press.
DOI: https://doi.org/10.2138/am-2020-7264. http://www.minsocam.org/

apply on all the points in the same way, it does not have any effect on the relative dispersion. Equation 8 gives the expected dispersion for single points measurements, and equation 9 for orthogonal couples. Here, D_{An}, "a" and N are the same as in equation 7, E_{Meas} is the measurement error, and E_{Tr} is the data treatment error.

Equation 8

$$D_{Th} = \sqrt{D_{An}^2 + E_{Meas}^2 + E_{Tr}^2} - \frac{a}{N-1}$$

Equation 9

$$D_{Th} = \sqrt{D_{An}^2 + \frac{E_{Meas}^2 + E_{Tr}^2}{2}} - \frac{a}{N-1}$$

The theoretical uncertainties follow a simple error propagation equation, which is expressed as shown in equation 10 for single points measurements, and equation 11 for orthogonal couples. Here, E_{Cor} plays a role on the final relative error and tends to account for most of the uncertainty when the number of points increases (see Figure 5).

Equation 10

$$E_{Th} = \sqrt{\frac{D_{An}^2 + E_{Meas}^2 + E_{Tr}^2}{N} + E_{Cor}^2}$$

Equation 11

$$E_{Th} = \sqrt{\frac{D_{An}^2 + \frac{E_{Meas}^2 + E_{Tr}^2}{2}}{N} + E_{Cor}^2}$$

Always consult and cite the final, published document. See http:/www.minsocam.org or GeoscienceWorld

Each of the above equations can be applied for both olivine and wadsleyite. All the parameters are displayed in Table 1.

It can be noted that all the dispersions and errors in this simulation neglect the initial asymmetry of the distribution of the OH/Si values (see distribution histograms in supplementary materials 3 and 4) which, although abnormal and strongly asymmetric (towards high values for single points measurements and low values for the orthogonal couples), rapidly tends toward a Gaussian-shaped distribution above 10 to 15 points. Moreover, the asymmetry of the distribution might be very difficult to observe on a real set of measurement because of the limited set of points in which the distribution of values may not have any statistical significance. Hence, the deviation caused by this hypothesis tends to be negligible above 10 to 15 measurement points, but very low number of points should still follow a very asymmetric distribution, increasing error.

It can be noted that the measurement and treatment errors have a very small effect on both the dispersion and the error (see Figure 5). On the other hand, power drift correction related errors (E_{Cor}) have a very strong effect on the final error, demonstrating that this step must be carefully performed in order to get correct values. An important result is that the use of averaged orthogonally polarized measurements roughly halves the theoretical dispersion of the values, thus decreasing the associated error. The total expected dispersion directly related to anisotropy (neglecting all the other error sources) for olivine is around ±29.4% for single points and ±14.8% for orthogonal couples. Wadsleyite displays slightly higher values, with 32.5% and 16.8% (all these values are shown in Table 1). The same effect could be reached on single points measurements with approximately four times more points. Another advantage of using the

Always consult and cite the final, published document. See http:/www.minsocam.org or GeoscienceWorld

orthogonal couples is that it forces to measure more diverse grain orientations in the sample, hence limiting the effect of a potential preferential crystallographic orientation within the sample.

To sum up, assuming a chemically homogeneous sample (in terms of water content), if the standard deviation is close to the expected dispersion (calculated with equations 8 or 9), the real analytical error is given by equations 10 or 11. It follows that, in the ideal case of randomly oriented crystals, the error on OH/Si for 5 to 10 measurement points is between 15 and 18% for single points, and 12 and 15% for orthogonal couples. A deviation inferior to the expected deviation (still assuming that the sample is homogeneous) would point out an insufficient sampling of the natural dispersion. A rough estimation of the real error in this case can be obtained with equation 12. Here, the difference between the expected deviation D_{Th} and the measured value D_{Smp} causes the final error (E_{Smp}) to increase from the ideal value E_{Th} to the total dispersion D_{Th}, equal to the error expected on a measurement based on one single measurement point.

In contrast, if the standard deviation is higher than D_{Th}, whether because the sample is heterogeneous or the measurements are too defective, the error "reduction" from D_{Smp} to E_{Smp} (from equations 8 or 9 to equations 10 or 11) may not be reasonable to apply directly. Considering that the sampling is sufficient in this case, an error approximation can be obtained from equation 10 (variables are the same as in equation 13).

Equation 12

$$E_{Smp} = D_{Th} - (D_{Th} - E_{Th}) \times \frac{D_{Smp}}{D_{Th}}$$

Always consult and cite the final, published document. See http:/www.minsocam.org or GeoscienceWorld

This is the peer-reviewed, final accepted version for American Mineralogist, published by the Mineralogical Society of America.
The published version is subject to change. Cite as Authors (Year) Title. American Mineralogist, in press.
DOI: https://doi.org/10.2138/am-2020-7264. http://www.minsocam.org/

Equation 13

$$E_{Smp} = \sqrt{\left(D_{Smp} \times \frac{E_{Th}}{D_{Th}}\right)^2 + \left(D_{Smp} - D_{Th}\right)^2}$$

Olivine and wadsleyite calibration lines

The water content of the samples used to build the calibration lines are shown in Table 2, along with the values of OH/Si measured with Raman spectroscopy. The calibration lines (see equation 14 and Figure 6) are built with least-square minimization, always pass by the origin, and take into account the effect of the water content uncertainties arising from FTIR and ERDA measurements as well as the Raman measurement. All the error bars on the OH/Si have been estimated with the method described above. Some samples thus display a relatively large error bar (such as 949 or M380b, see Figure 6 and Table 2) because the measured dispersion was significantly greater than the expected dispersion (obtained from equations 8 to 11). On the other hand, some samples, such as M382, displayed a very low dispersion that may be related to insufficient sampling, once again resulting in a larger error bar. The factor to convert from OH/Si to ppm in weight of water (F in equation 11) is 93108±24005 for olivine, 250868±45591 for wadsleyite (with iron), and 57546±13916 for wadsleyite (without iron). This result shows the tremendous effect of iron on the spectrum's shape and intensity, implying that chemical composition has to be verified in order to quantify the water content of wadsleyite. There are two identified causes to this difference, the first being that for two samples with comparable water contents, the Si area of an iron-free wadsleyite displays sharper peaks, even if their heights are comparable, implying a lower Si intensity. However, at the same time, its OH area is more intense. This causes the OH/Si of an iron-free wadsleyite to be much higher than the one of an

Always consult and cite the final, published document. See http:/www.minsocam.org or GeoscienceWorld

This is the peer-reviewed, final accepted version for American Mineralogist, published by the Mineralogical Society of America.
The published version is subject to change. Cite as Authors (Year) Title. American Mineralogist, in press.
DOI: https://doi.org/10.2138/am-2020-7264. http://www.minsocam.org/

iron-bearing wadsleyite with a comparable water content (see supplementary materials 5). Figure 6 displays the calibration lines for olivine and wadsleyite.

Equation 14

$$C_{H_2O}(ppm\ wt) = F \times \frac{\mathrm{OH}}{\mathrm{Si}}_{Smp\ Norm}$$

The uncertainty on the slope obtained for each calibration has to be added to the final error E_{Smp} described above, the total uncertainty on the water content being given by equation 15, where E_{H2O} is the total error, E_{Smp} is the total relative error on the OH/Si of the sample, and E_{Cal} is the calibration-related relative error. The same can be applied to dispersions.

Equation 15

$$E_{H_2O} = \sqrt{E_{Smp}^2 + E_{Cal}^2}$$

The uncertainty on the slope of the calibration line (as shown in Figure 6) arising from the errors in water quantification of the standards and from the error on their OH/Si *often* becomes the major component of the total uncertainty on the water content compared to the error on the measurement of OH/Si with Raman spectroscopy.

Regarding olivine, the 26% uncertainty on the calibration line is much larger than the 12% error on the OH/Si measurement attained for a large number of points (in the case of orthogonal couples, see Figure 5). Following equation 15, this 12% error (E_{Smp}) increases to 29% only because of the uncertainty on the calibration (E_{Cal}). The same problem applies to wadsleyite with the 18% error on the calibration line for iron-bearing wadsleyite and the 24% error for iron-

Always consult and cite the final, published document. See http:/www.minsocam.org or GeoscienceWorld

This is the peer-reviewed, final accepted version for American Mineralogist, published by the Mineralogical Society of America.
The published version is subject to change. Cite as Authors (Year) Title. American Mineralogist, in press.
DOI: https://doi.org/10.2138/am-2020-7264. http://www.minsocam.org/

free wadsleyite. The greater is the error on the OH/Si of the sample (because of insufficient sampling or sample heterogeneities), the smaller the contribution of calibration uncertainties to the total error will be (see Figure 7).

DISCUSSION

The quantification of as much error and uncertainty sources as possible provides a better understanding of the data dispersion inherent to the use of Raman spectroscopy on anisotropic crystals. The relative impact of each source of error highlights what affects the more the final error, showing where further progress and developments could be made. The first issue is the laser-drift during and between different sessions. The method used to overcome this problem brings an additional source of error (referred as E_{Cor} throughout this study), as it implies two OH/Si ratio measurements on a standard glass, thus adding twice data treatment and measurement error to the result (divided by $\sqrt{2}$, as the value measured is supposed to be the same for the two measurements). Moreover, as this correction has to be applied on all the points of a sample, its contribution to the total error does not decrease with an increasing number of points. Consequently, its relative contribution increases, and becomes the major part of the error on the OH/Si ratio above around 20 to 25 single points, or 5 orthogonal couples (see Figure 5). This power-drift correction error is also responsible for a significant part of the calibration error, thus acting in two different ways in the final error. On the other hand, insufficient sampling of the natural dispersion rapidly causes the final error to be larger than the measured dispersion (see equation 11). Orthogonally polarized averaged measurements, improving by force the sampling of various orientations (and thus, anisotropy) help to prevent from orientation biases.

Secondly, the effect of the calibration uncertainty (caused by the errors on each standard point) on the final error acts similarly as the power-drift correction uncertainty (both are

Always consult and cite the final, published document. See http:/www.minsocam.org or GeoscienceWorld

This is the peer-reviewed, final accepted version for American Mineralogist, published by the Mineralogical Society of America.
The published version is subject to change. Cite as Authors (Year) Title. American Mineralogist, in press.
DOI: https://doi.org/10.2138/am-2020-7264. http://www.minsocam.org/

458 insensitive to the number of points), rapidly becoming the major part of the error, particularly for
459 olivine. Focusing on the ideal case where the dispersion observed on the sample (D_{Smp}) equals the
460 theoretical dispersion (D_{Th}), implying that E_{Smp} and E_{Th} are equal, the conversion factors D_{H2O}/
461 E_{H2O} (following equation 15, and applying this to the dispersion by replacing E_{Smp} with D_{Smp} to
462 obtain D_{H2O}) and D_{Smp}/E_{Smp} of wadsleyite are superior to those of olivine in all cases (except for
463 two points in the orthogonal couples case, see Figure 7). This is caused by the higher effect of the
464 error sources on D_{Th} than on E_{Th} in the case of wadsleyite, where E_{Cor} mitigates their effect, hence
465 increasing D_{Smp}/E_{Smp}. Adding E_{Cal} does not change this observation, except that it mitigates these
466 effects, lowering the expected "gain" on errors, with higher attenuation for higher E_{Cal} (see Figure
467 7). In the case of a poor sampling, accounting for E_{Cal} tends to mitigate the effect of the error
468 augmentation (see equation 9) by increasing E_{Smp} to a much higher E_{H2O}, lowering the effect of
469 equation 15.

470 Water content heterogeneities may cause the measured dispersion to be larger than the
471 expected one. In such cases, when the ratio of observed over expected dispersion is close to one,
472 even if the gain may seem high, it is important to consider that chemical heterogeneities should
473 remain as low as possible (see the discussion around equation 13). The present water
474 quantification method by Raman spectroscopy relies on the hypothesis that only the orientation
475 varies from one crystal to another, and that these orientations are distributed randomly and
476 uniformly. This means that chemically heterogeneous samples (should it be a major element
477 content variation, or in water content variation) are unsuitable for precise water quantification
478 with this method. In the case of wadsleyite, we observed that the iron content has a tremendous
479 effect on the calibration line slope, implying that composition has to be measured to verify if all
480 the analyzed crystals have a similar iron content. The problem of the random distribution of

Always consult and cite the final, published document. See http:/www.minsocam.org or GeoscienceWorld

This is the peer-reviewed, final accepted version for American Mineralogist, published by the Mineralogical Society of America.
The published version is subject to change. Cite as Authors (Year) Title. American Mineralogist, in press.
DOI: https://doi.org/10.2138/am-2020-7264. http://www.minsocam.org/

orientations in samples also has to be considered, as preferential orientation may occur in some samples. However, if a sample is chemically homogeneous, a sample with a strong disparity of orientations could be identified if it displays values dispersion much smaller than the expected dispersion (see discussion around equation 12).

CONCLUSION

Raman spectroscopy allows the water content measurement of samples of any size above few micrometers, and with water contents down to 150-200 ppm in weight (see Bolfan-Casanova et al. 2014), with no observed upper limit, where many other methods may require large samples, or are unsuitable for very high water contents (FTIR). Even if vibrational spectroscopy is very useful to discriminate OH point defects over contamination, the sensitivity to crystallographic orientation in anisotropic samples often leads to high standard deviations in the measurements of water content (Férot and Bolfan-Casanova 2012). Here we show that a large part of this dispersion may be related to the natural anisotropy of the measured mineral, and is thus normal. The main objective of this work was to be able to calculate the error associated to the measurement of water content in olivine and wadsleyite, using Raman spectroscopy, knowing the anisotropy of the OH/Si ratio for each phase. We identified throughout this study various sources of error. The major parameters (beside anisotropy) affecting errors on the final values are the uncertainties on the calibration line, insufficient sampling of anisotropy, and the laser-drift correction errors. Nevertheless, most of the errors obtained with this procedure fall in a range of 20-25% of relative error for wadsleyite, and 25-30% for olivine, making Raman spectroscopy still suitable for quantification water content in olivine and wadsleyite. The detailed study of the error sources has provided a greater understanding of the method, and has allowed an

Always consult and cite the final, published document. See http:/www.minsocam.org or GeoscienceWorld

This is the peer-reviewed, final accepted version for American Mineralogist, published by the Mineralogical Society of America.
The published version is subject to change. Cite as Authors (Year) Title. American Mineralogist, in press.
DOI: https://doi.org/10.2138/am-2020-7264. http://www.minsocam.org/

503 improvement of the treatment methods, reducing significantly the uncertainties arising from this
504 part of the procedure.

505 ## IMPLICATIONS

506 The high spatial resolution of Raman spectroscopy allows the study of water distribution
507 among different phases of fine polymineralic samples of complex (natural) composition, with a
508 wide range of measurable water contents. Although relatively high, the uncertainties on water
509 concentration are sufficiently low to infer the effect of thermodynamic intensive parameters on
510 water incorporation. The method proposed here can also be applied to all orthorhombic minerals.

511 ## ACKNOWLEDGMENTS

512 The authors thank Jean-Louis Fruquière and Cyrille Guillot for their help and advises on
513 the experimental assemblies, István Kovács, Anthony Withers, and Mainak Mookherjee for very
514 precise and helpful reviews of this manuscript, Federica Schiavi and Arnaud Guillin for fruitful
515 discussions, and Laurent Jouffret for the time spent on the orientation attempt of the wadsleyite
516 single crystal with X-ray diffraction. The multi-anvil apparatus of Laboratoire Magmas et
517 Volcans is financially supported by the CNRS (Instrument national de l'INSU). This is
518 Laboratory of Excellence ClerVolc contribution N° 419.

519 ## REFERENCES

520 Ardia, P., Hirschmann, M.M., Withers, A.C., and Tenner, T.J. (2012) H2O storage capacity of
521 olivine at 5–8 GPa and consequences for dehydration partial melting of the upper mantle.
522 Earth and Planetary Science Letters, 345-348, 104-116.

Always consult and cite the final, published document. See http:/www.minsocam.org or GeoscienceWorld

This is the peer-reviewed, final accepted version for American Mineralogist, published by the Mineralogical Society of America.
The published version is subject to change. Cite as Authors (Year) Title. American Mineralogist, in press.
DOI: https://doi.org/10.2138/am-2020-7264. http://www.minsocam.org/

523 Asimow, P.D., Stein, L.C., Mosenfelder, J.L., and Rossman, G.R. (2006) Quantitative polarized
524 infrared analysis of trace OH in populations of randomly oriented mineral grains.
525 American Mineralogist, 91, 278-284.

526 Bali, E., Bolfan-Casanova, N., and Koga, K.T. (2008) Pressure and temperature dependence of H
527 solubility in forsterite: An implication to water activity in the Earth interior. Earth and
528 Planetary Science Letters, 268, 354-363.

529 Bell, D.R., and Rossman, G.R. (1992) Water in Earth's mantle: The role of nominally anhydrous
530 minerals. Science, 255, 1391-1397.

531 Bell, D.R., Rossman, G.R., Maldener, J., Endisch, D., and Rauch, F. (2003) Hydroxide in olivine:
532 A quantitative determination of the absolute amount and calibration of the IR spectrum.
533 Journal of Geophysical Research, 108, 2105.

534 Bolfan-Casanova, N., Montagnac G. and Reynard B. (2014) Measurements of water contents in
535 olivine using Raman spectroscopy. American Mineralogist 99, 149-156.

536 Bolfan-Casanova N., Schiavi, F., Novella, D., Bureau, H., Raepsaet, C., Khodja, H., and
537 Demouchy S. (2018) Examination of Water Quantification and Incorporation in
538 Transition Zone Minerals Wadsleyite, Ringwoodite and Phase D Using ERDA (Elastic
539 Recoil Detection Analysis). Frontiers in Earth Science, 6, 75.

540 Demouchy, S., and Bolfan-Casanova, N. (2016) Distribution and transport of hydrogen in the
541 lithospheric mantle: A review. Lithos, 240-243, 402-425.

Always consult and cite the final, published document. See http:/www.minsocam.org or GeoscienceWorld

This is the peer-reviewed, final accepted version for American Mineralogist, published by the Mineralogical Society of America.
The published version is subject to change. Cite as Authors (Year) Title. American Mineralogist, in press.
DOI: https://doi.org/10.2138/am-2020-7264. http://www.minsocam.org/

542 Férot, A., and Bolfan-Casanova, N. (2012) Water storage capacity in olivine and pyroxene to 14
543 GPa: Implications for thewater content of the Earth's upper mantle and nature of seismic
544 discontinuities. Earth and Planetary Science Letters, 349-350, 218-230.

545 Fischer, G.W., and Medaris, L.G. (1969) Cell dimensions and X-ray determinative curve for
546 synthetic Mg-Fe olivines. American Mineralogist, 54, 741-753.

547 Inoue, T., Yurimoto, H., and Kudoh, Y. (1995) Hydrous modified spinel, Mg1.75SiH0.5O4: A
548 new water reservoir in the mantle transition region. Geophysical Resaerch Letters, 22,
549 issue 2, 117-120.

550 Ishibashi, H., Arakawa, M., Ohi, S., Yamamoto, J., Miyake, A., and Kagi, H. (2008) Relationship
551 between Raman spectral pattern and crystallographic orientation of a rock-forming
552 mineral: a case study of Fo89Fa11 olivine. Journal of Raman Spectroscopy, 39, 1653-
553 1659.

554 Jacobsen, S.D, Demouchy, S., Frost, D.J., Boffa Ballaran, T., and King, J. (2005) A systematic
555 study of OH in hydrous wadsleyite from polarized FTIR spectroscopy and single-crystal
556 X-ray diffraction: Oxygen sites for hydrogen storage in Earth's interior. American
557 Mineralogist, 90, 61-70.

558 Koga, K., Hauri, E., Hirschmann, M.M., and Bell, D. (2003) Hydrogen concentration analyses
559 using SIMS and FTIR: Comparison and calibration for nominally anhydrous minerals.
560 Geochemistry Geophysics Geosystems, 4, number 2, 1019.

561 Kohlstedt, D.L., Keppler, H., and Rubie, D.C. (1996) Solubility of water in the α, β and γ phases
562 of (Mg,Fe)2SiO4. Contributions to Mineralogy and Petrology, 123, 345-357.

Always consult and cite the final, published document. See http:/www.minsocam.org or GeoscienceWorld

This is the peer-reviewed, final accepted version for American Mineralogist, published by the Mineralogical Society of America.
The published version is subject to change. Cite as Authors (Year) Title. American Mineralogist, in press.
DOI: https://doi.org/10.2138/am-2020-7264. http://www.minsocam.org/

563 Kovács, I., Hermann, J., O'Neill, H.S.C., Fitz Gerald, J., Sambridge, M., and Horváth, G. (2008)
564 Quantitative absorbance spectroscopy with unpolarized light: Part II. Experimental
565 evaluation and development of a protocol for quantitative analysis of mineral IR spectra.
566 American Mineralogist, 93, 765-778.

567 Kovács, I., O'Neill, H.S.C., Hermann, J. and Hauri, E.H. (2010) Site-specific infrared O-H
568 absorption coefficients for water substitution into olivine. American Mineralogist 95, 292-
569 299.

570 Libowitzky, E., and Rossman, G.R. (1996) Principles of quantitative absorbance measurements in
571 anisotropic crystals. Physics and Chemistry of Minerals, 23, 319-327.

572 Litasov, K.D., Shatskiy, A., and Ohtani, E. (2014) Melting and subsolidus phase relations in
573 peridotite and eclogite systems with reduced C–O–H fluid at 3–16GPa. Earth and
574 Planetary Science Letters, 391, 87-99.

575 Mercier, M., Di Muro, A., Giordano, D., Métrich, N., Lesne, P., Pichavant, M., Scaillet, B.,
576 Clocchiatti, R., Montagnac, G. (2009) Influence of glass polymerisation and oxidation on
577 micro-Raman water analysis in alumino-silicate glasses. Geochimica et Cosmochimica
578 Acta, 73, 197-217.

579 Mosenfelder, J.L., Le Voyer, M., Rossman, G.R., Guan, Y., Bell, D.R., Asimow, P.D., and Eiler,
580 J.M. (2011) Analysis of hydrogen in olivine by SIMS: Evaluation of standards and
581 protocol. American Mineralogist, 96, 1725-1741.

582 Novella, D., Frost, D.J., Hauri, E.H., Bureau, H., Raepsaet, C., and Roberge, M. (2014) The
583 distribution of H2O between silicate melt and nominally anhydrous peridotite and the

Always consult and cite the final, published document. See http:/www.minsocam.org or GeoscienceWorld

This is the peer-reviewed, final accepted version for American Mineralogist, published by the Mineralogical Society of America.
The published version is subject to change. Cite as Authors (Year) Title. American Mineralogist, in press.
DOI: https://doi.org/10.2138/am-2020-7264. http://www.minsocam.org/

584 onset of hydrous melting in the deep upper mantle. Earth and Planetary Science Letters,
585 400, 1-13.

586 Peslier, A.H. (2010) A review of water contents of nominally anhydrous natural minerals in the
587 mantles of Earth, Mars and the Moon. Journal of Volcanology and Geothermal Research,
588 197, 239-258.

589 Qiu, Y., Jiang, H., Kovács, I., Xia, Q.K. and Yang, X. (2018) Quantitative analysis of H-species
590 in anisotropic minerals by unpolarized infrared spectroscopy: An experimental evaluation.
591 American Mineralogist, 103, 1761-1769.

592 Schiavi, F., Bolfan-Casanova, N., Withers, A.C., Médard, E., Laumonier, M., Laporte, D.,
593 Flaherty, T., and Gómez-Ulla, A. (2018) Water quantification in silicate glasses by
594 Raman spectroscopy: Correcting for the effects of confocality, density and ferric iron.
595 Chemical Geology, 483, 312-331.

596 Smyth, J.S., and Keppler, H., Eds. (2006) Water in nominally anhydrous minerals. Reviews in
597 Mineralogy and Geochemistry, 62.

598 Tenner, T.J., Hirschmann, M.M., Withers, A.C., and Ardia, P. (2012) H2O storage capacity of
599 olivine and low-Ca pyroxene from 10 to 13 GPa: consequences for dehydration melting
600 above the transition zone. Contributions to Mineral Petrology, 163, 297-316.

601 Thomas, S.M., Thomas, R., Davidson, P., Reichart, P., Koch-Müller, M., and Dollinger, G.
602 (2008) Application of Raman spectroscopy to quantify trace water concentrations in
603 glasses and garnets. American Mineralogist, 93, 1550-1557.

Always consult and cite the final, published document. See http:/www.minsocam.org or GeoscienceWorld

Thomas, S.M., Jacobsen, S.D., Bina, C.R., Reichart, P., Moser, M., Hauri, E.H., Koch-Müller, M., Smyth, J.R., and Dollinger, G. (2015) Quantification of water in hydrous ringwoodite. Frontiers in Earth Sciences, 2, 38.

Thomas, S.M., Wilson, K., Koch-Müller, M., Hauri, E.H., McCammon, C., Jacobsen, S.D., Lazarz, J., Rhede, D., Ren, M., Blair, N., and Lenz, S. (2015) Quantification of water in majoritic garnet. American Mineralogist, 100, 1084-1092.

Weis, F.A., Lazor, P., and Skogby, H. (2018) Hydrogen analysis in nominally anhydrous minerals by transmission Raman spectroscopy. Physics and Chemistry of Minerals, 45, 597-607.

Withers, A.C., and Hirschmann, M.M. (2007) H2O storage capacity of MgSiO3 clinoenstatite at 8-13 GPa, 1100-1400°C. Contributions to Mineralogy and Petrology, 154, 663-674.

Withers, A.C., and Hirschmann, M.M. (2008) Influence of temperature, composition, silica activity and oxygen fugacity on the H2O storage capacity of olivine at 8 GPa. Contributions to Mineralogy and Petrology, 156, 595-605.

Withers, A.C., Bureau, H., Raepsaet, C., and Hirschmann, M.M. (2012) Calibration of infrared spectroscopy by elastic recoil detection analysis of H in synthetic olivine. Chemical Geology, 334, 92-98.

Withers, A.C. (2013) On the use of unpolarized infrared spectroscopy for quantitative analysis of absorbing species in birefringent crystals. American Mineralogist, 98,689–697

Always consult and cite the final, published document. See http:/www.minsocam.org or GeoscienceWorld

This is the peer-reviewed, final accepted version for American Mineralogist, published by the Mineralogical Society of America.
The published version is subject to change. Cite as Authors (Year) Title. American Mineralogist, in press.
DOI: https://doi.org/10.2138/am-2020-7264. http://www.minsocam.org/

623 Yang, X. (2016) Effect of oxygen fugacity on OH dissolution in olivine under peridotite-
624 saturated conditions: An experimental study at 1.5-7 GPa and 1100-1300°C. Geochimica
625 et Cosmochimica Acta, 173, 319-336.

626 Yoshino, T., Nishihara, Y., Karato, S. ichiro (2007) Complete wetting of olivine grain boundaries
627 by a hydrous melt near the mantle transition zone. Earth and Planetary Science Letters,
628 256, 466-472

629 Zarei, A., Klumbach, S., and Keppler, H. (2016) The relative Raman scattering cross sections of
630 H_2O and D_2O, with implications for in situ studies of isotope fractionation. ACS Earth
631 and Space Chemistry, 2, 925-934.

632

Always consult and cite the final, published document. See http:/www.minsocam.org or GeoscienceWorld

This is the peer-reviewed, final accepted version for American Mineralogist, published by the Mineralogical Society of America.
The published version is subject to change. Cite as Authors (Year) Title. American Mineralogist, in press.
DOI: https://doi.org/10.2138/am-2020-7264. http://www.minsocam.org/

633 Table 1: Fitting parameters (D_{An} and a) and estimated error sources values (E) for
634 dispersion and error equations (equations 6 to 13). D_{An} is the calculated anisotropy contribution to
635 the observed values deviation; E_{Meas} is the measurement related error, E_{Tr} the treatment related
636 error, and E_{Cor} the laser-drift correction related error.

	Olivine		Wadsleyite	
	Single points	**Orthogonal couples**	**Single points**	**Orthogonal couples**
D_{An}	28.1	14.1	32.5	16.8
a	6	3	6.74	3.37
E_{Meas}	4.44	4.44	4.25	4.25
E_{Tr}	3.58	3.58	3.82	3.82
E_{Cor}	11.9	11.9	11.9	11.9

637

Always consult and cite the final, published document. See http:/www.minsocam.org or GeoscienceWorld

This is the peer-reviewed, final accepted version for American Mineralogist, published by the Mineralogical Society of America.
The published version is subject to change. Cite as Authors (Year) Title. American Mineralogist, in press.
DOI: https://doi.org/10.2138/am-2020-7264. http://www.minsocam.org/

638 Table 2: Standards used for the olivine and wadsleyite calibrations of OH/Si versus H_2O
639 concentration in ppm by weight of water. Wadsleyite* standards are iron-free. Raman
640 measurement type "1" refers to the case of single point measurement and "2" to the case of
641 orthogonal couples.

		Source measurement			Raman measurement			
Sample	**Phase**	**Method**	**ppm wt H_2O**	**error**	**Type**	**Points**	**OH/Si**	**error**
949	Olivine	FTIR	1304	290	1	8	0.01534	0.00371
M497	Olivine	ERDA	750	38	1	10	0.00405	0.00081
M589	Olivine	FTIR	1244	596	1	57	0.01127	0.00141
1033	Olivine	FTIR	522	176	2	11	0.00806	0.00118
895b	Olivine	FTIR	180	21	2	12	0.00382	0.00156
1044b	Olivine	FTIR	1766	674	2	10	0.01924	0.00250
M817	Olivine	FTIR	640	215	2	10	0.00350	0.00103
M818	Olivine	FTIR	291	72	2	10	0.00269	0.00104
M230	Wadsleyite	ERDA	1045	52	1	10	0.01591	0.00270
M226A	Wadsleyite	ERDA	4209	210	2	12	0.03863	0.00642
M380b	Wadsleyite	ERDA	12206	610	1	10	0.04219	0.01833
M382	Wadsleyite	ERDA	27271	1364	2	13	0.10122	0.01864
M226B	Wadsleyite*	ERDA	4000	200	2	10	0.10574	0.01457
2053	Wadsleyite*	ERDA	21600	1080	1	10	0.46945	0.10382
2054	Wadsleyite*	ERDA	34000	1700	1	10	0.49357	0.07957

642

Always consult and cite the final, published document. See http:/www.minsocam.org or GeoscienceWorld

This is the peer-reviewed, final accepted version for American Mineralogist, published by the Mineralogical Society of America.
The published version is subject to change. Cite as Authors (Year) Title. American Mineralogist, in press.
DOI: https://doi.org/10.2138/am-2020-7264. http://www.minsocam.org/

643 **FIGURE CAPTIONS**

644 Figure 1 : Optical image of the olivine and wadsleyite samples used for the anisotropy
645 quantification.

646

647 Figure 2 : Raman spectra of olivine (grey) and wadsleyite (black) in the silicate region
648 and the OH region. The wide bars underneath each graph (light bar for olivine, dark bar for
649 wadsleyite) depict the integration window used for water quantification. The darker short lines
650 depict the anchor point area used for baseline correction. The baseline shape is linear for olivine
651 Si area, and cubic for OH area, and is polylinear for wadsleyite Si area, and cubic for OH area.

652

653 Figure 3 : OH/Si values of olivine (top) and wadsleyite (bottom) as a function of the
654 orientation of the crystal relative to the beam, for three perpendicular faces. Error bars are the
655 estimated uncertainties linked to measurement errors and data treatment (see text). Horizontal
656 error bars are an estimation of the angle's error. Solid and dashed lines (M) represent the fitted
657 curves obtained through equation 3 (or 4 for wadsleyite). Olivine crystallographic faces were
658 identified, whereas for wadsleyite, faces are named arbitrarily (F1, F2 and F3).

659

660 Figure 4 : Three-dimensional plot of OH/Si values of olivine (as fitted in Figure 3) as a
661 function of crystallographic orientation. Values obtained with incident beam parallel to the *a* axis
662 are displayed in the (100) (bc) plane, and so on for the other faces. Grey points (which due to

Always consult and cite the final, published document. See http:/www.minsocam.org or GeoscienceWorld

their density may be displayed as light grey lines here) are the extrapolations of the solid lines (derived from Figure 3) for any given orientation (see equation 5).

Figure 5 : Simulated relative dispersions (empty circles) and errors (solid circles) for olivine (top) and wadsleyite (bottom), for the case of single point measurements (left) and orthogonal couples (right), expressed in percent deviation from the average. Light grey symbols stand for the contribution of anisotropy *(An)* alone. Adding the measurement *(Meas)* uncertainties yields the intermediate grey symbols (mostly hidden by the dark grey ones). Adding treatment *(Tr)* uncertainties gives the dark grey symbols, and finally adding the uncertainty arising from the power correction *(Cor)* yields the black circles.

Figure 6 : Calibration lines for olivine (top), iron-bearing wadsleyite (center) and iron-free wadsleyite (bottom). The straight line corresponds to the fitted value. The dashed and dotted lines show the 1σ and 2σ uncertainties respectively.

Figure 7 : Dispersion over error ratio (D/E) as a function of the number of points, for analytical uncertainties only (grey circles and discs, representing D_{Smp} and E_{Smp}), and for total uncertainty, including calibration related uncertainty (black circles and discs, for D_{H2O} and E_{H2O}). Full circles represent the ideal case where $D_{Smp} = D_{Th}$ (ideal sampling), thin circles represent the insufficient sampling case (here, D_{Smp} is 75% of D_{Th}), and thick circles represent the case of a dispersion D_{Smp} 50% superior to D_{Th}.

Always consult and cite the final, published document. See http:/www.minsocam.org or GeoscienceWorld

Figure 1

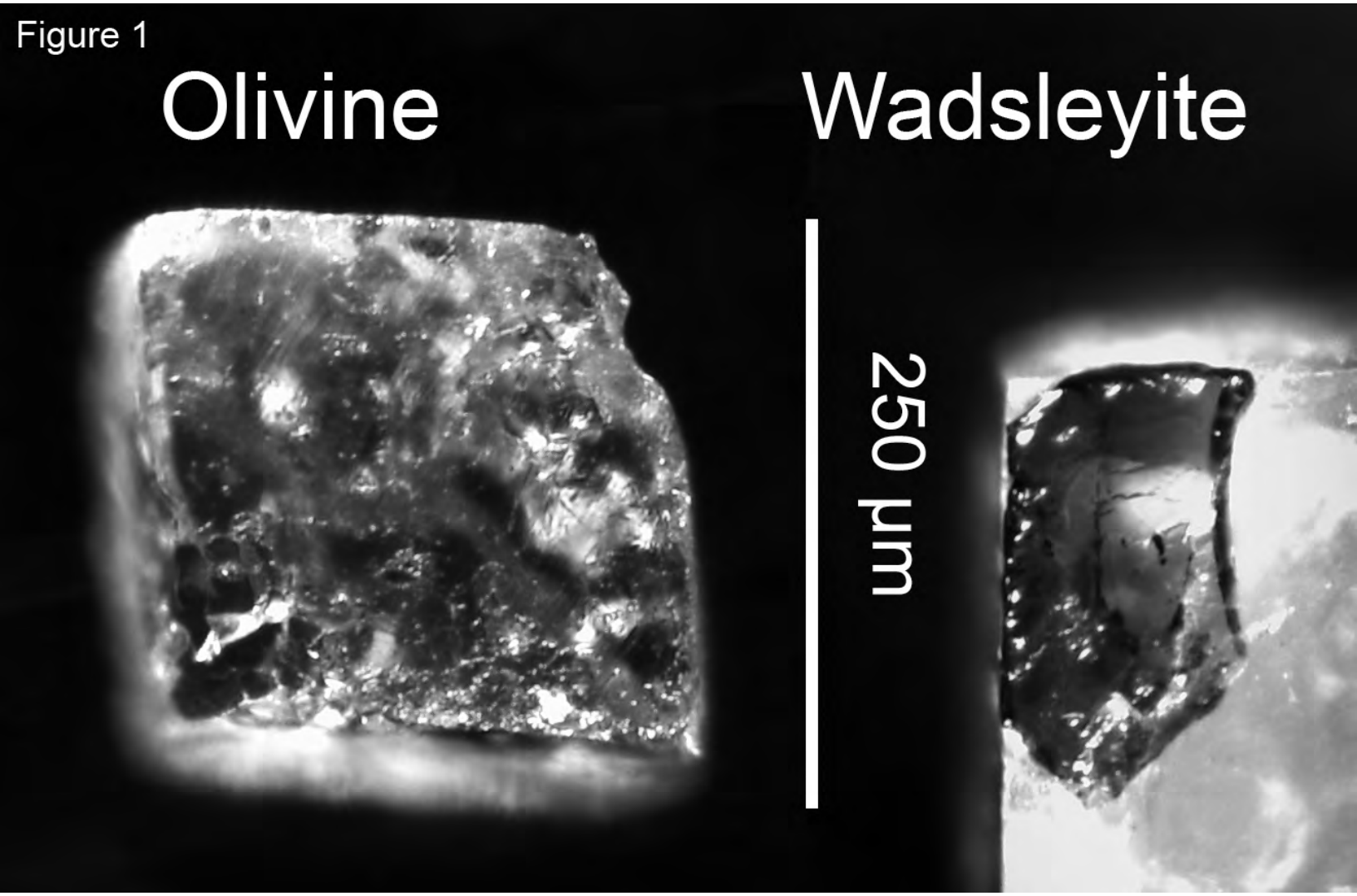

Figure 2

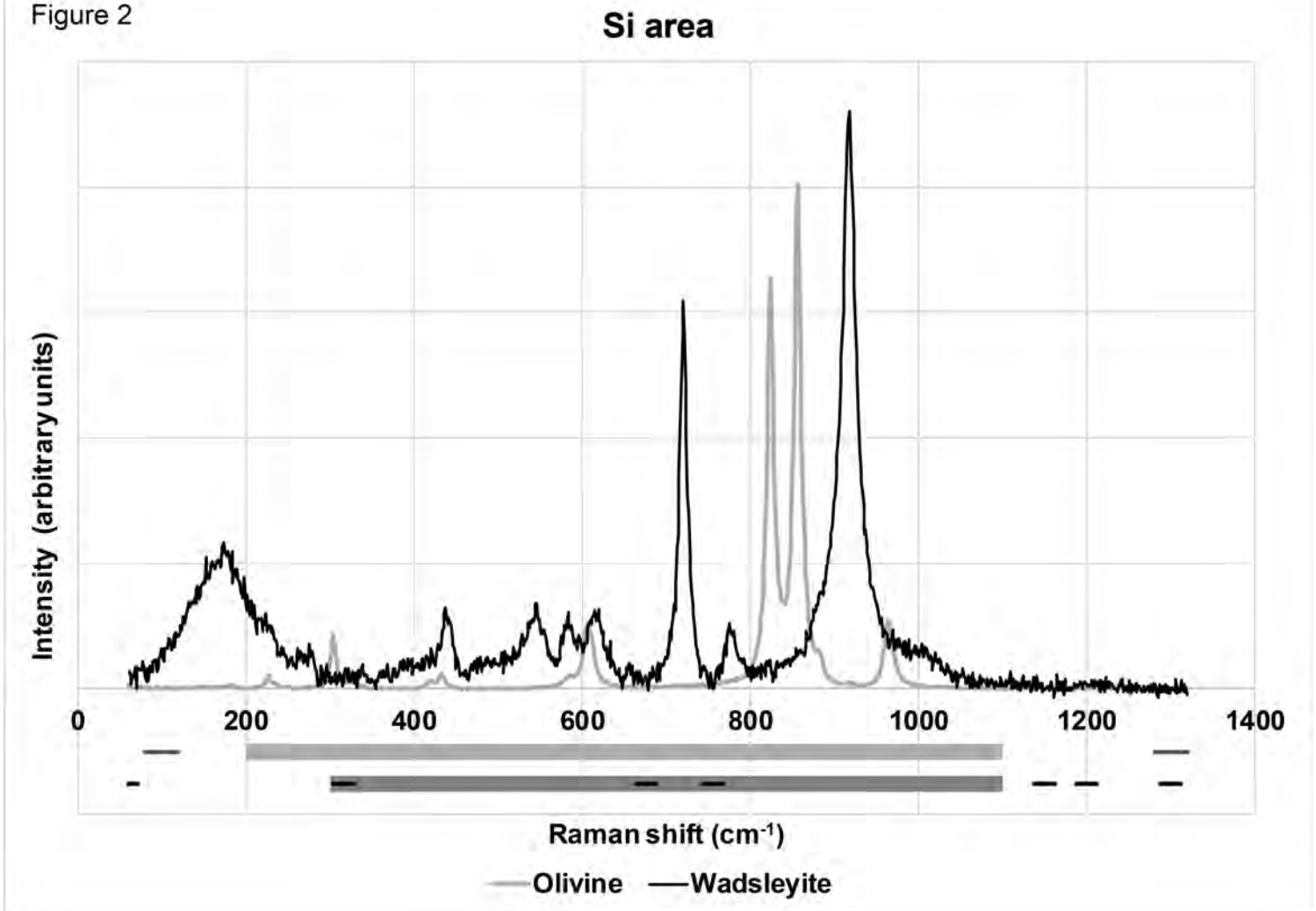
Si area
Intensity (arbitrary units)
0
200
400
600
800
1000
1200
1400
Raman shift (cm-1)
Olivine
Wadsleyite

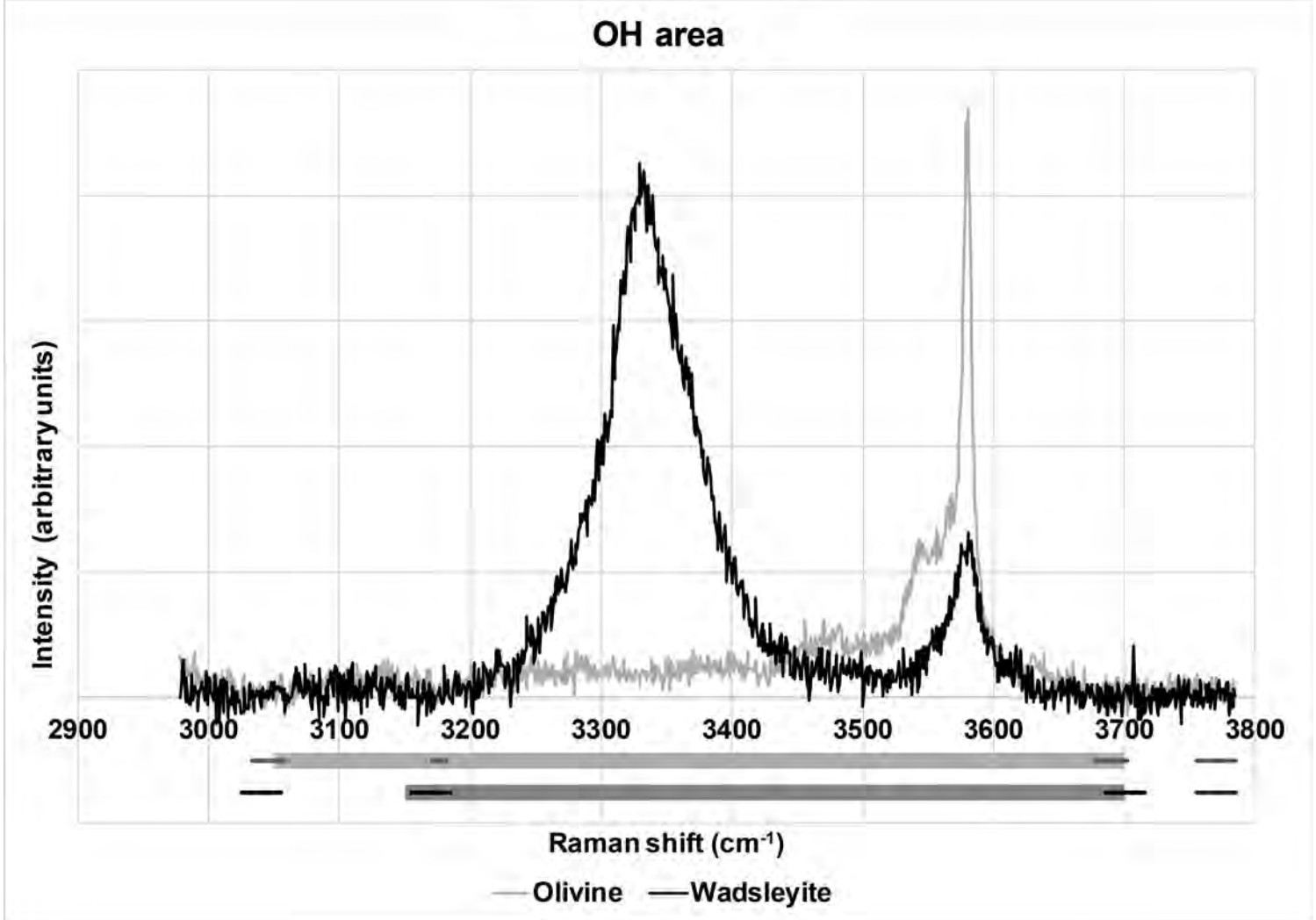
OH area
Intensity (arbitrary units)
2900
3000
3100
3200
3300
3400
3500
3600
3700
3800
Raman shift (cm-1)
Olivine
Wadsleyite

Figure 3

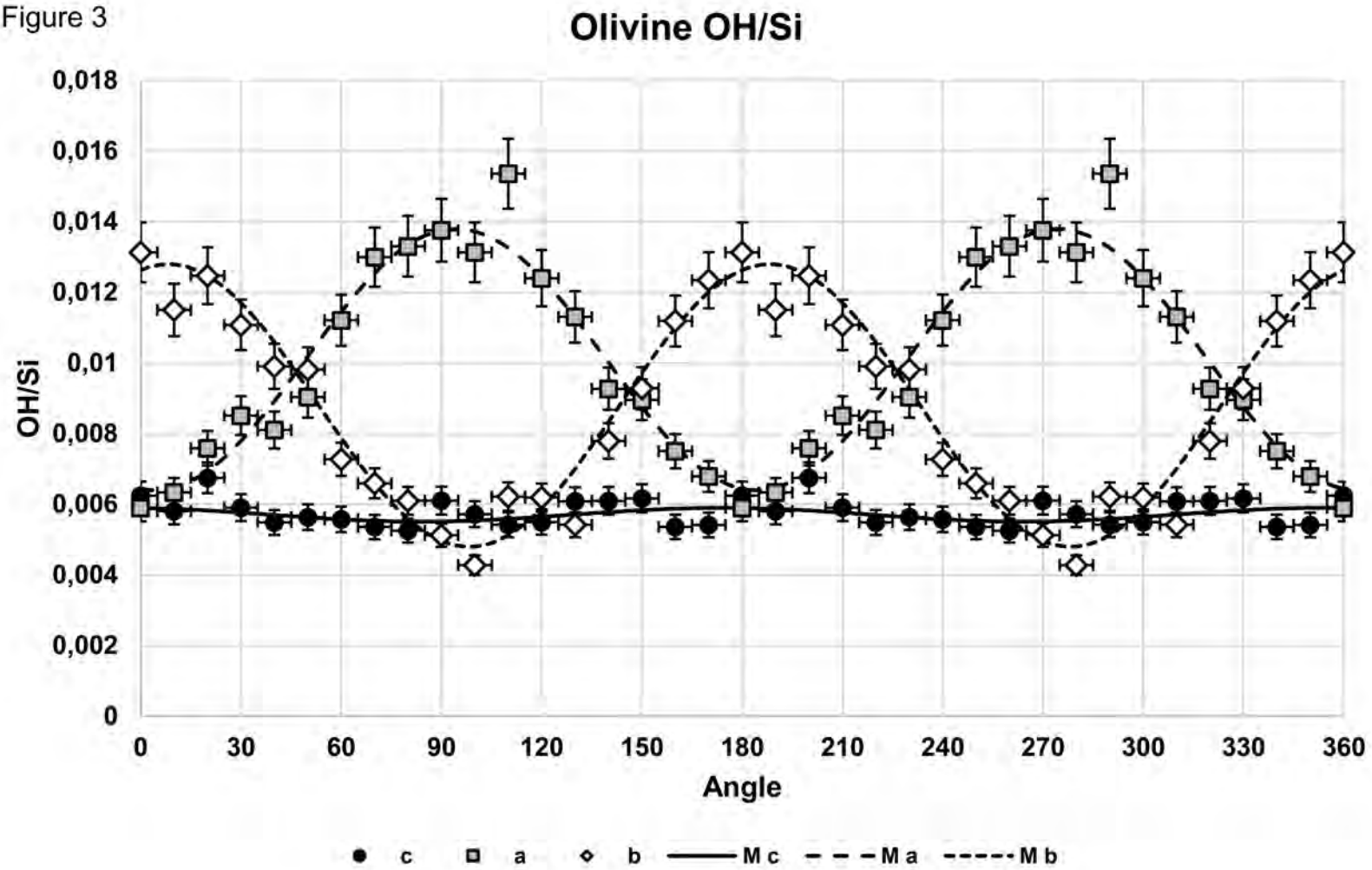
Olivine OH/Si
0,018
0,016
0,014
0,012
0,01
0,008
0,006
0,004
0,002
0
OH/Si
0
30
60
90
120
150
180
210
240
270
300
330
360
Angle
c
a
b
M c
M a
M b

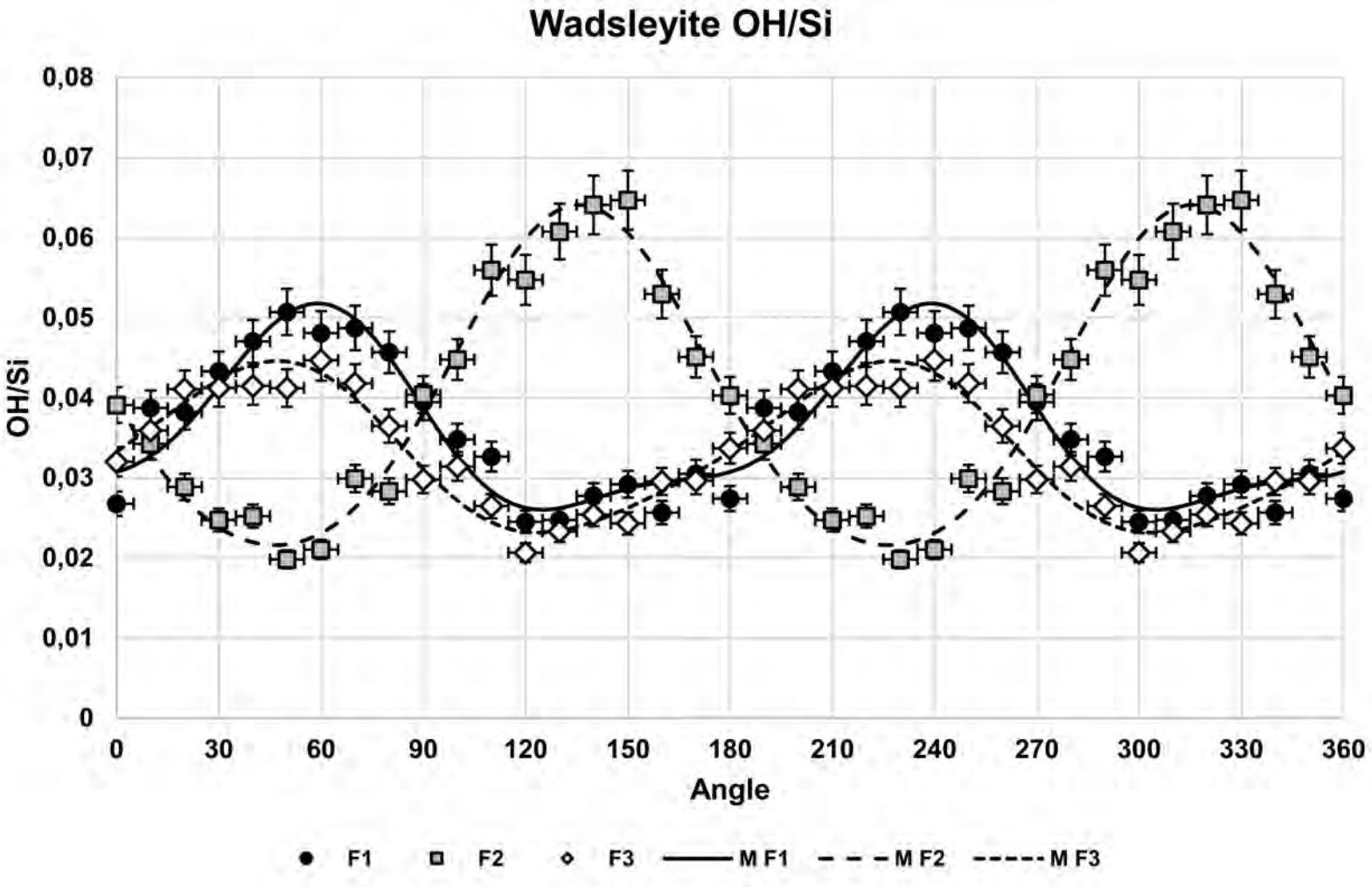
Wadsleyite OH/Si
0,08
0,07
0,06
0,05
0,04
0,03
0,02
0,01
0
OH/Si
0
30
60
90
120
150
180
210
240
270
300
330
360
Angle
F1
F2
F3
M F1
M F2
M F3

Figure 4

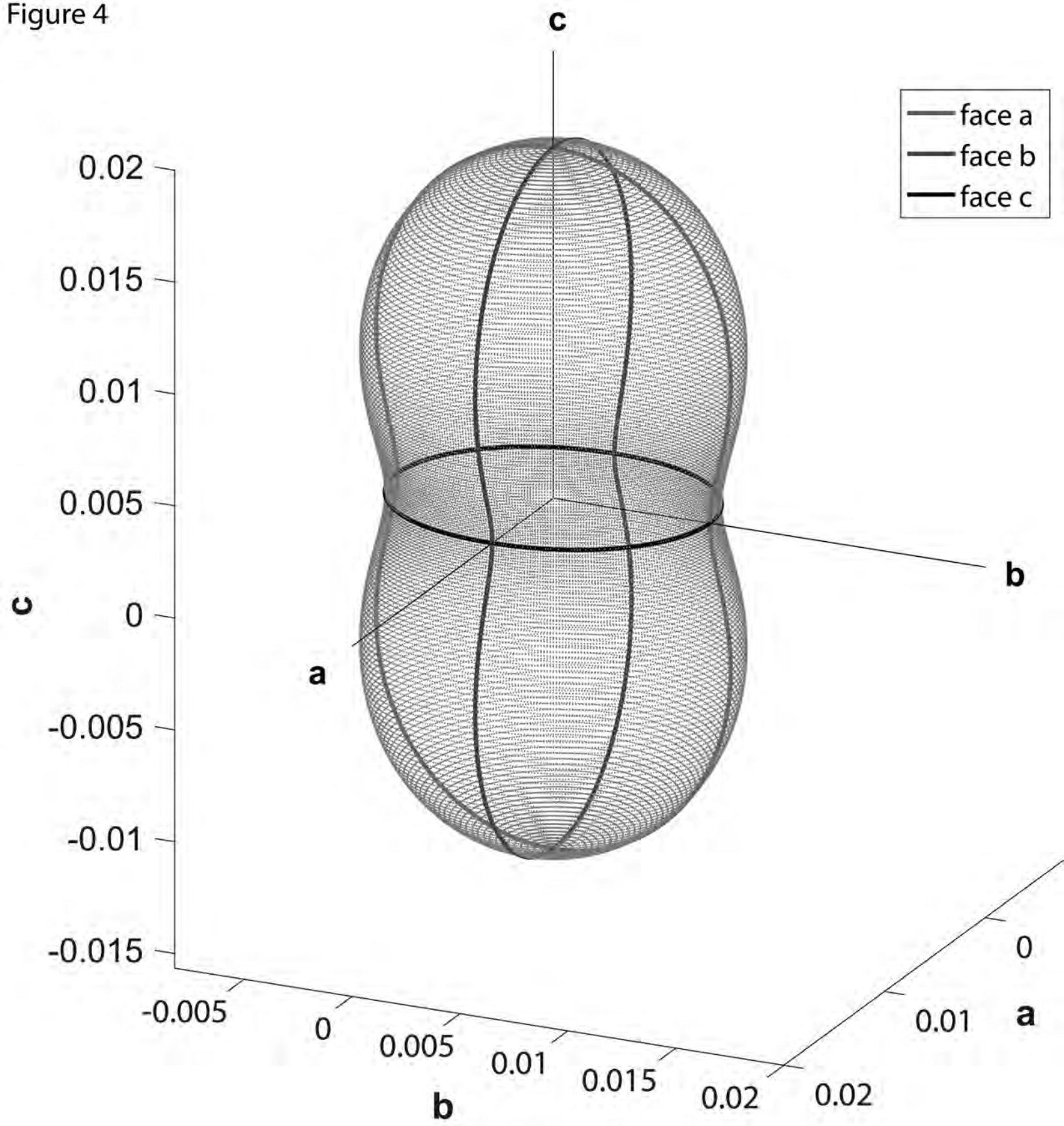
c
face a
face b
face c
0.02
0.015
0.01
0.005
0
-0.005
-0.01
-0.015
c
b
a
-0.005
0
0.005
0.01
0.015
0.02
b
0.02
0.01
0
a

Figure 5

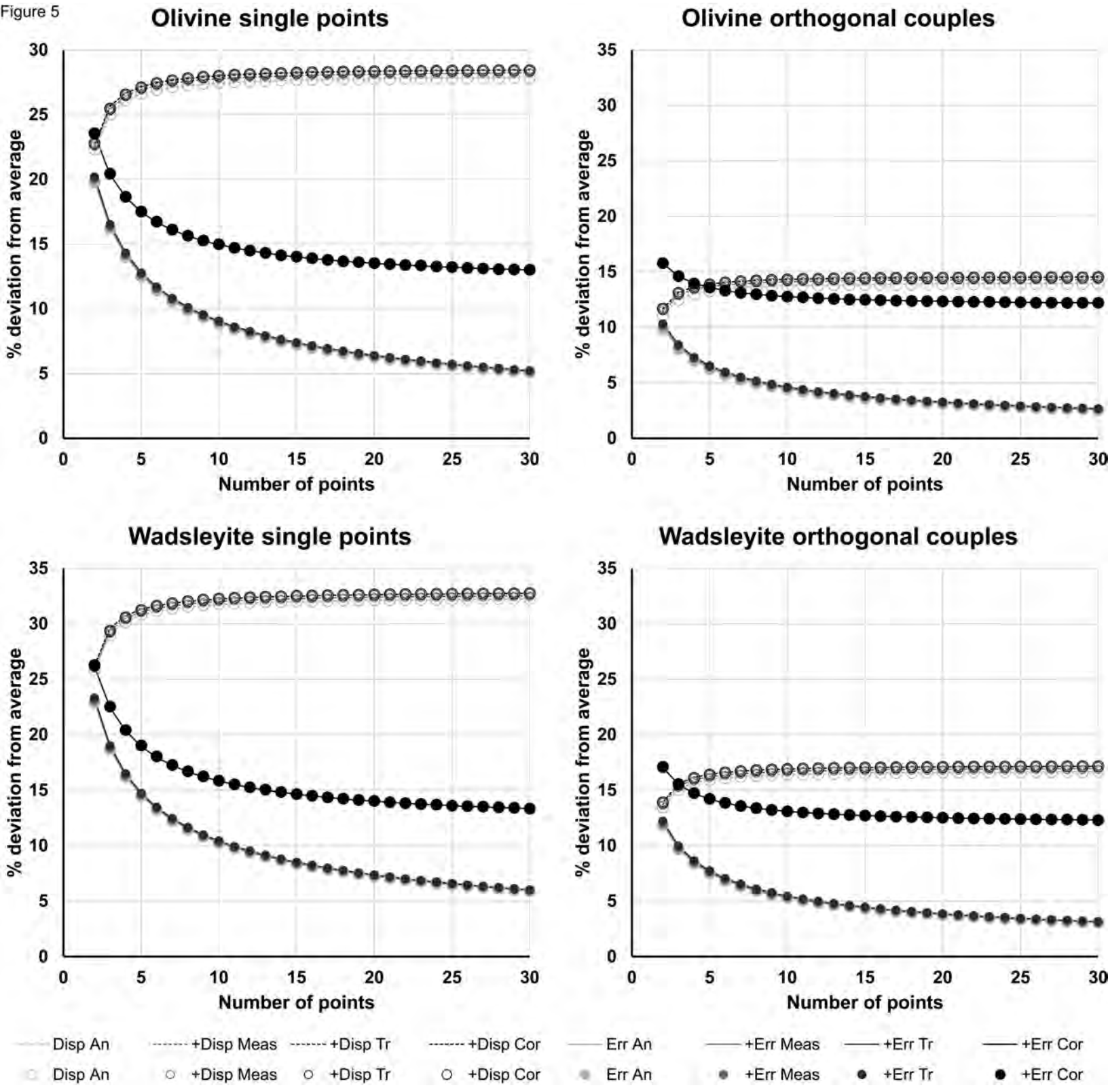
Olivine single points
% deviation from average
Number of points
Olivine orthogonal couples
% deviation from average
Number of points
Wadsleyite single points
% deviation from average
Number of points
Wadsleyite orthogonal couples
% deviation from average
Number of points
Disp An
+Disp Meas
+Disp Tr
+Disp Cor
Err An
+Err Meas
+Err Tr
+Err Cor

Figure 6

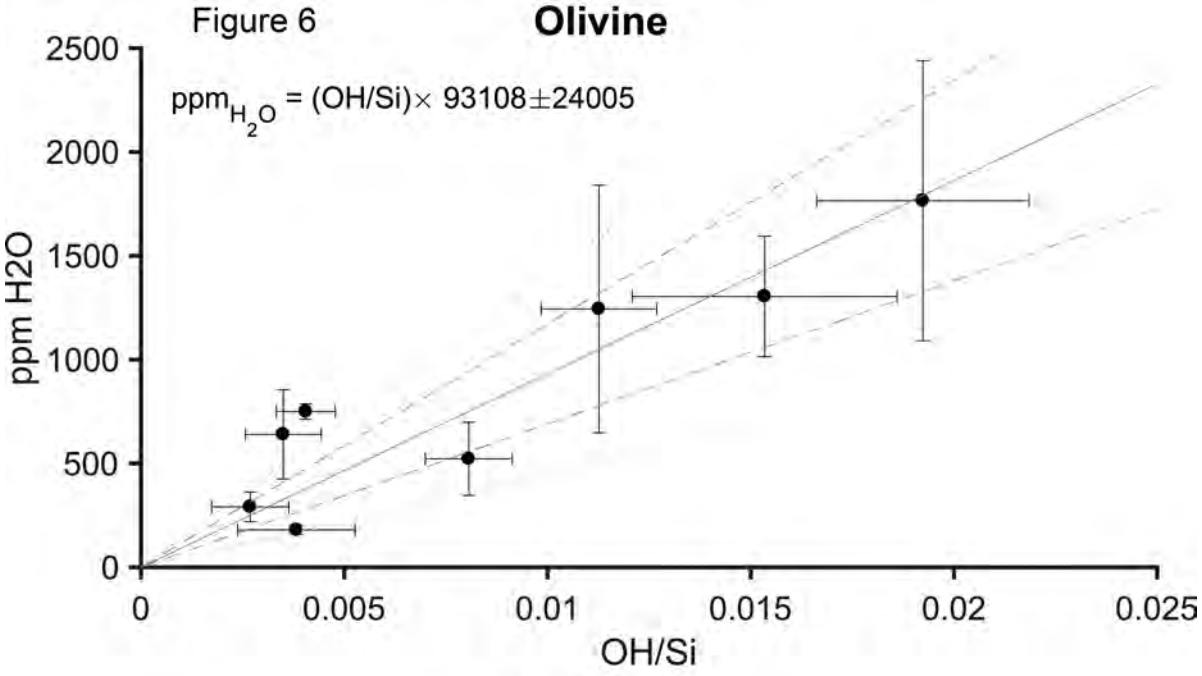
Olivine
ppm$_{H_2O}$ = (OH/Si)× 93108±24005
ppm H2O
OH/Si
0
500
1000
1500
2000
2500
0.005
0.01
0.015
0.02
0.025

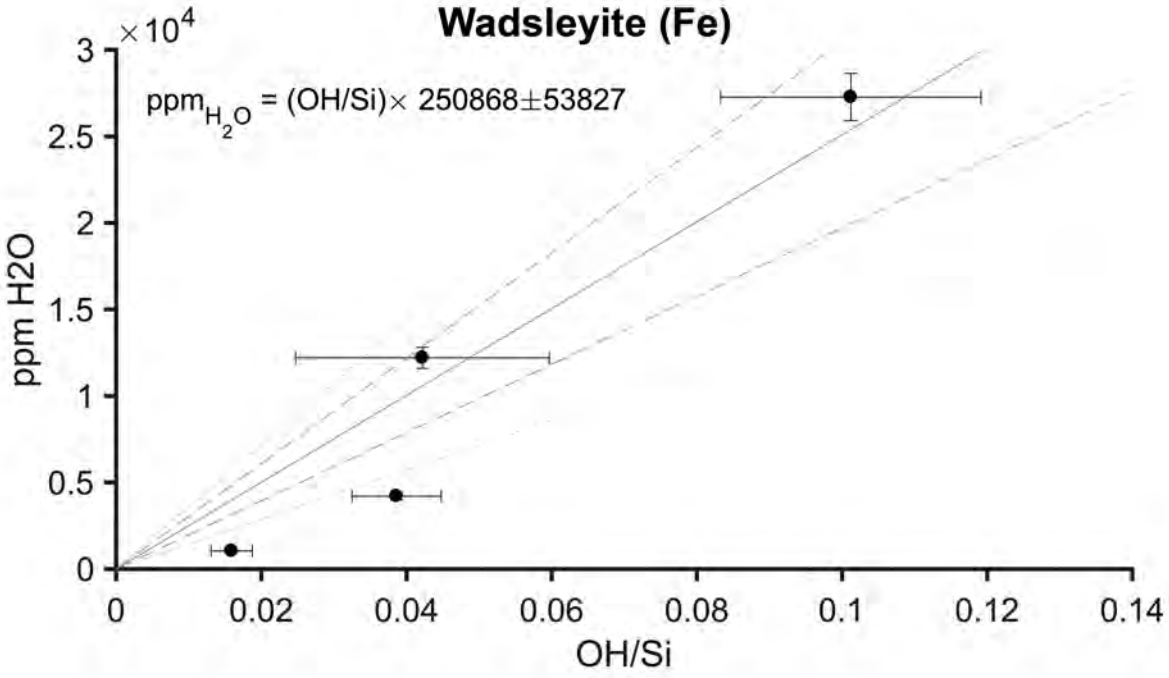
Wadsleyite (Fe)
×10^4
ppm$_{H_2O}$ = (OH/Si)× 250868±53827
ppm H2O
OH/Si
0
0.5
1
1.5
2
2.5
3
0.02
0.04
0.06
0.08
0.1
0.12
0.14

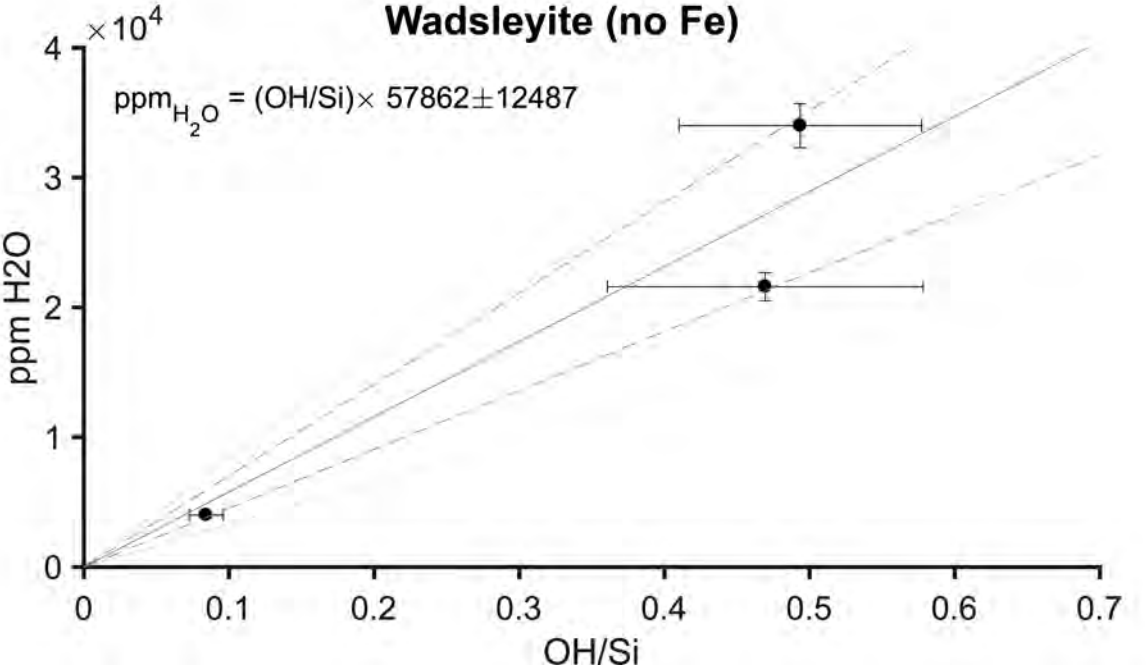
Wadsleyite (no Fe)
×10^4
ppm$_{H_2O}$ = (OH/Si)× 57862±12487
ppm H2O
OH/Si
0
1
2
3
4
0.1
0.2
0.3
0.4
0.5
0.6
0.7

Figure 7

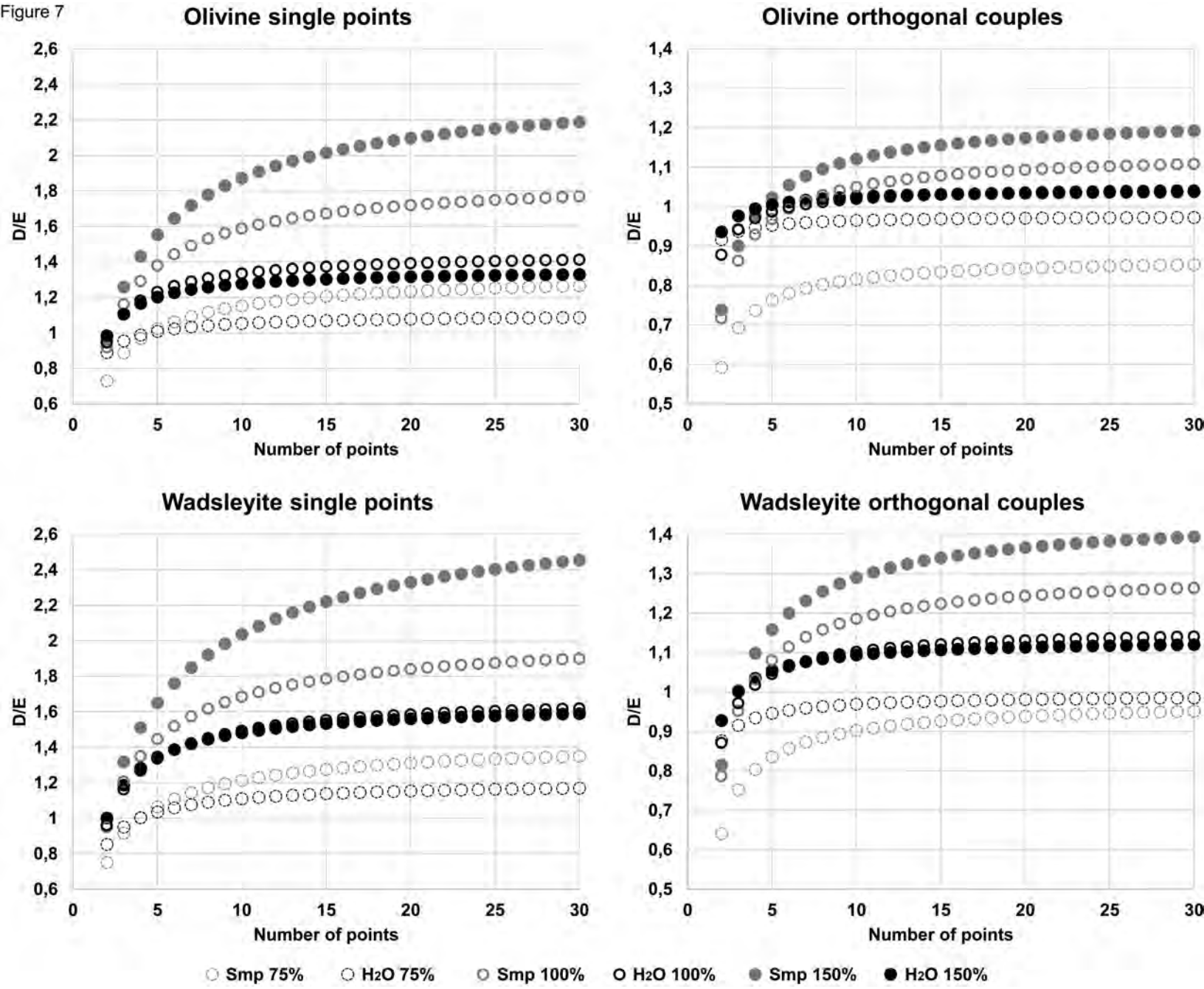
Olivine single points
D/E
Number of points
Olivine orthogonal couples
D/E
Number of points
Wadsleyite single points
D/E
Number of points
Wadsleyite orthogonal couples
D/E
Number of points
Smp 75%
H2O 75%
Smp 100%
H2O 100%
Smp 150%
H2O 150%